Frequency and Magnitude Analysis of the Macro-instability Related Component of the Tangential Force Affecting Radial Baffles in a Stirred Vessel

P. Hasal, J. Kratěna, I. Fořt

Experimental data obtained by measuring the tangential component of force affecting radial baffles in a flat-bottomed cylindrical mixing vessel stirred with pitched blade impellers is analysed. The maximum mean tangential force is detected at the vessel bottom. The mean force value increases somewhat with decreasing impeller off-bottom clearance and is noticeably affected by the number of impeller blades. Spectral analysis of the experimental data clearly demonstrated the presence of its macro-instability (MI) related low-frequency component embedded in the total force at all values of impeller Reynolds number. The dimensionless frequency of the occurrence of the MI force component is independent of stirring speed, position along the baffle, number of impeller blades and liquid viscosity. Its mean value is about 0.074. The relative magnitude (Q_{MI}) of the MI-related component of the total force is evaluated by a combination of proper orthogonal decomposition (POD) and spectral analysis. Relative magnitude Q_{MI} was analysed in dependence on the frequency of the impeller revolution, the axial position of the measuring point in the vessel, the number of impeller blades, the impeller off-bottom clearance, and liquid viscosity. Higher values of Q_{MI} are observed at higher impeller off-bottom clearance height and (generally) Q_{MI} decreases slightly with increasing impeller speed. The Q_{MI} value decreases in the direction from vessel bottom to liquid level. No evident difference was observed between 4 blade and 6 blade impellers. Liquid viscosity has only a marginal impact on the Q_{MI} value.

Keywords: stirred vessel, baffles, tangential force, macro-instability, spectral analysis, proper orthogonal decomposition.

1 Introduction

Liquid flow in mechanically stirred vessels has been studied intensively on recent decades. Numerous theoretical and experimental studies have been performed concerning various aspects of liquid flow in stirred vessels, e.g., mean flow velocity, intensity of turbulence, energy dissipation rate or spatial and temporal scales of a turbulent velocity field, etc. Liquid flow in a stirred vessel operated under steady operational conditions may be considered as a pseudo--stationary high-dimensional dynamical system constituted by hierarchically ordered unsteady flows (vortices and eddies). The temporal and spatial scales of these flows span several decimal orders of magnitude. Recently, a pseudo-periodic large-scale flow has been identified in stirred vessels occurring with very low frequency and manifesting itself on spatial scales comparable to the size of the mixing vessel [1–10]. This flow was named *macro-instability* (MI) *of the flow pattern*, and its existence has been confirmed by a special mechanical measuring device [7], by laser-Doppler velocimetry (LDV) [8–10], and by visual observations [11, 12].

The presence of MI in the flow pattern is typically displayed by a distinct peak in the low-frequency part of the power spectrum of the local liquid velocity or other liquid flow-related experimental data. Comprehensive reviews of a broad spectrum of experimentally observed phenomena related to macro-instability were given in our previous papers [13,14]. Macro-instability of the flow pattern has a strong impact on mixing processes closely linked to fluid motion, e.g., on local mass- and heat-transport rates [4], local gas hold-up [1], homogenisation rate, etc. Bittorf and Kresta [15] identified the macro-instability of the flow pattern as a mechanism responsible for liquid mixing outside the active volume of the primary liquid circulation loop. Macro-instability, however, also exerts strong forces affecting solid surfaces immersed in stirred liquid, e.g., baffles, draft tubes, cooling and heating coils, etc. These forces may significantly affect the performance of the mixing vessel and, in certain cases, can even cause serious failures of the equipment.

An axially located pitched blade impeller in a standard cylindrical mixing vessel equipped with radial baffles exhibits two main force effects: axial and tangential. The axial force affects radial baffles only very slightly. Conversely, it is the tangential force that exhibits most of the dynamic pressure affecting them. The vertical distribution (along the baffle) of the dynamic pressure was measured in a standard mixing vessel by Kratěna et al [16–18] over a wide interval of impeller Reynolds number value and in dependence on the impeller off-bottom clearance height. The force effects of two types of impellers were studied: pitched blade impellers with four or six blades and the standard Rushton turbine. Strong qualitative differences in the vertical distribution of the mean tangential force and of its variance were observed. Pitched blade impellers elicit maximum force at the vessel bottom, and the magnitude of the force gradually falls in the direction towards the liquid level. Rushton turbine impellers produce maximum force at the impeller level and the force rapidly decays in both the below-impeller and above-impeller region.

Few attempts have been reported in the literature [19, 20] to separate the deterministic and stochastic components of

mixing phenomena in stirred tanks. Letellier et al [19] adopted a Hilbert transform based procedure for separating the low-dimensional deterministic part of an experimental time series. Kovacs et al [20] used the Fourier transform for the same purpose. Recently we have established a new technique for detecting the macro-instability of the flow pattern from local velocity data, evaluating its relative magnitude and reconstructing its temporal evolution [13, 14, 21]. The technique is based on a combination of spectral analysis with proper orthogonal decomposition [22–26], and in this paper we apply this technique to experimental data obtained by Kratěna et al [16–18] by measuring the tangential component of the force exerted on radial baffles by the liquid flow in a mixing vessel in order to quantify the relative magnitude of its macro-instability related component, to analyse its vertical distribution in the vessel and the effects of the frequency of the impeller revolution, the number of impeller blades and the liquid viscosity. The frequency of occurrence of macro-instability related force component is also analysed.

2 Experimental

A cylindrical flat-bottomed vessel with four radial baffles was used in all experiments reported in this paper. The dimensions of the vessel and of the impellers are marked in Fig. 1 and their values are listed in Table 1. Two pitched blade impellers with six and four blades (pitch angle 45°) were used for stirring. The impellers pumped the liquid towards the bottom of the vessel.

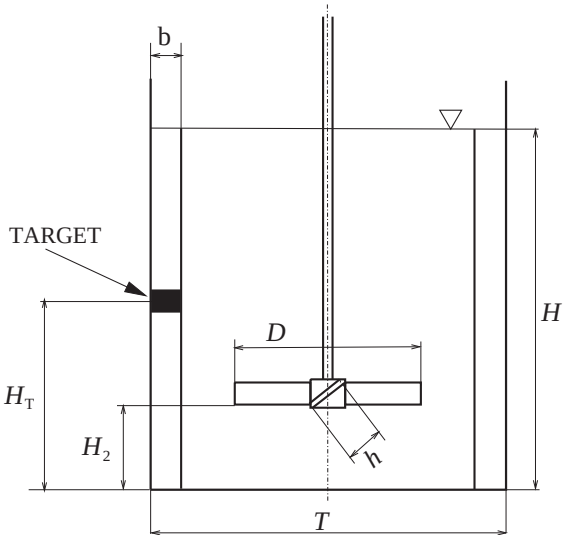

Fig. 1: Mixing vessel geometry

Water and hot and cold aqueous glycerine solutions (with viscosity 3 and 6 mPas, respectively) were used as working liquids in order to extend the experimentally attainable interval of impeller Reynolds number values. The frequency of impeller rotation f_M was varied from 5 s^{-1} to 9.17 s^{-1}. The corresponding interval of Re_M values was (approximately) from 16000 to 83300.

The tangential force affecting the baffles was measured by means of a trailing target (target height $h_T = 10$ mm, target width $B = 28$ mm) located in a slit made in the baffle and enabled to rotate around an axis parallel to the vessel axis. The target was balanced by a couple of (calibrated) springs, and its angular displacement was scanned via a photo-electronic sensor (see Kratěna et al [16–18] for details of the measuring equipment). The sampling period was $T_S = 20$ ms. The signal from the sensor was recorded on a PC (after A/D conversion) and subsequently used for evaluation of the tangential force $\{F_i, i = 1, \ldots, N_S\}$ affecting the target. The duration of a single experiment was 20 minutes and $N_S \approx 60000$ samples was typically stored.

Table 1: Dimensions of mixing vessel and impeller

Dimension	Value
Vessel diameter	$T = 0.3$ m
Liquid aspect ratio	$H/T = 1$
Impeller to tank diameter ratio	$D/T = 0.333$
Relative impeller off-bottom clearance	$H_2/T = 0.20$ and 0.35
Measuring target relative axial position	$H_T/H = 0$; 0.1; 0.2; 0.35; 0.5; 0.65; 0.8
Relative baffle width	$b/T = 0.1$
Relative impeller blade width	$h/D = 0.2$
Number of impeller blades	$N_B = 4$ and 6

Finally, the force F_i was converted to dimensionless force according to the relation

$$F_i^* = \frac{F_i}{\rho f_M^2 D^4} \tag{1}$$

The time series of F_i^* values measured at seven distinct locations H_T/H of the target along the baffle (see Table 1) were used for analysis. At each target height, the value of Re_M was varied over the entire attainable interval. The total number of processed data sets was 335.

3 Numerical analysis of experimental data

The numerical procedures used for experimental data analysis are described only briefly, as details can be found either in the original papers [22–26] or in our previous reports [13, 14, 21].

The power spectra of the time records of the measured tangential force were used to detect the presence of the component generated by the macro-instability of the flow pattern. The power spectral densities were evaluated by means of an algorithm based on the fast Fourier transform [27]. Examples of power spectra of the analysed data are shown in Fig. 3. The peaks located at dimensionless frequency $f/f_M \approx 0.075$ clearly demonstrate the presence of an MI-related component of the total measured force at all impeller Reynolds number values. The value of the dimensionless

frequency of the MI-related peak ($f/f_M \approx 0.075$) agrees very well with the findings of other authors and of our previous studies, which were, however, based on entirely different experimental data (local liquid velocity) [7–10, 13, 14, 21].

A procedure based on an application of the proper orthogonal decomposition (POD) technique was used for extracting the MI-related low-frequency component from the experimental data. Details of the procedure can be found in our previous papers [13,14,21], and the general principles of POD are described elsewhere [22]. First, the raw data, i.e., the time series $\{F_i^*, i = 1, \ldots, N_S\}$ recorded at a given measuring point, is centred by subtracting the mean force value F_m^*

$$\Phi_i^* = F_i^* - F_m^*, \quad i = 1, \ldots, N_S . \tag{2}$$

Then, the so called N-window [24–26] is applied to the centred data series $\{\Phi_i^*, i = 1, \ldots, N_S\}$. The N-window extracts N consecutive elements from the series $\{\Phi_i^*\}$ to vector $\{\mathbf{\Phi}_k^*\}$

$$\mathbf{\Phi}_k^* = \left[\Phi_j^*,\ j = k, \ldots, k + N - 1\right],\ k = 1, \ldots, N_S - (N - 1) \tag{3}$$

The set of vectors $\{\mathbf{\Phi}_k^*, k = 1, \ldots, m-(N-1)\}$ resulting from repeated application of the N-window to the centred velocity data is then rearranged to a form of the so called trajectory matrix $\mathbf{W}$

$$\mathbf{W} = \left[\mathbf{\Phi}_1^*, \mathbf{\Phi}_2^*, \ldots, \mathbf{\Phi}_{N_S-(N-1)}^*\right]^T . \tag{4}$$

Autocovariance matrix $\mathbf{R}$ of the trajectory matrix $\mathbf{W}$ is then evaluated by matrix multiplication

$$\mathbf{R} = \mathbf{W}\,\mathbf{W}^T \tag{5}$$

and its (non-negative) eigenvalues α_k and eigenvectors $\mathbf{V}_k$, $k = 1, \ldots, N$ are then determined by any proper algorithm, e.g., by singular value decomposition [27]. The eigenvalues α_k sorted in decreasing order form a so called spectrum of POD eigenvalues, and each α_k value expresses the magnitude of the contribution of the k-th eigenmode to the total analysed signal. The eigenvectors $\mathbf{V}_k$ are used for evaluating the eigenmodes $a_k(t)$ of the original data series $\{F_i^*\}$ using the relation

$$a_k(t) = (\mathbf{W} \cdot \mathbf{V}_k), \tag{6}$$

where $(\cdot)$ denotes the inner product. The eigenmodes are functions of only time and are often called *chronos* [24]. The eigenmodes $a_k(t)$ can be used for reconstructing the temporal evolution of the macro-instability related component of the data

$$F_{MI}^*(t_j) = F_m^* + \sum_{K_{MI}} R_{1,K_{MI}} a_{K_{MI}}(t_j),\ j = 1, \ldots, N_S - N . \tag{7}$$

The summation in Eq. (7) is performed over a set of selected values of the index K_{MI}: the power spectra of the eigenmodes $a_k(t)$ are evaluated first. Then only eigenmodes with a single significant peak in their power spectra, located exactly at the macro-instability frequency f_{MI} (cf. Fig. 7), are summed in Eq. (7), and thus the MI-related phenomenon is reconstructed. More details on eigenmode selection and the summation procedure can be found in our previous papers [13,14,21]. The eigenvalues α_k are used for evaluating the relative magnitude Q_{MI} of the macro-instability related component of the tangential force affecting the baffles

$$Q_{MI} = \frac{\sum_{j \in K_{MI}} \alpha_j}{\sum_{j=1}^{N} \alpha_j} \tag{8}$$

The summation in the numerator on the right hand side of Eq. (8) is performed over the same K_{MI} values as in Eq. (7).

4 Results and Discussion

First, the vertical distribution of the magnitude and the variability of the dimensionless tangential force affecting the baffle in the mixing vessel was analysed. The mean values F_m^* were evaluated for each moving target location H_T/H and mixing vessel configuration used in the experiments (the configuration is specified by the number of impeller blades N_B and by the impeller off-bottom clearance height H_2/H). Averaging of the tangential force values was performed over all Re_M values used at a given target location and vessel configuration, i.e., the values measured at different impeller speeds f_M and at different liquid viscosities were averaged. The results are shown in Fig. 2. This figure also shows the standard deviation of the dimensionless tangential force resulting from the averaging procedure (error bars). The standard deviation characterises the variability of the value of F_m^* due to the varying Re_M value. It is obvious that the distribution of mean tangential force F_m^* along the baffle is qualitatively the same for all configurations of the mixing vessel. The force attains its maximum at the vessel bottom and then decreases to a minimum located slightly above the impeller position. The minima attain negative values, i.e., the direction of the liquid flow and the resulting force is reverted at their positions compared to the flow at the vessel bottom. The rapidity of the decrease in the mean force value is somewhat higher for impellers located closer to the vessel bottom ($H_2/H = 0.2$). In the upper part of the vessel ($H_T/H \geq 0.5$) the mean force gradually increases back to positive values that are, however, considerably lower than the force values recorded at the vessel bottom. The mean tangential force affecting the baffles is generally lower at higher values of the impeller off-bottom clearance height, i.e., at $H_2/H = 0.35$ (panels b) and d) in Fig. 2), and for the four blade impeller (panels c) and d) in Fig. 2). The variability of the mean tangential force (error bars in Fig. 2) decreases from the bottom to the top of the mixing vessel for all vessel configurations. The variability of the tangential force is particularly profound at the vessel bottom and in the adjacent below-impeller region, i.e., in the region where the baffles are affected by the impeller discharge stream. The effects of the impeller rotation speed and of the liquid viscosity are suppressed in the above-impeller region, i.e., in the ascending liquid stream, where the tangential force is generally weak.

Spectral analysis of the experimental time series data was performed in order to detect the macro-instability related component of the total tangential force embedded in the data. The analysis clearly demonstrates the presence of distinct peaks in the low-frequency part ($f/f_M < 0.1$) of the power spectra for all vessel configurations and all impel-

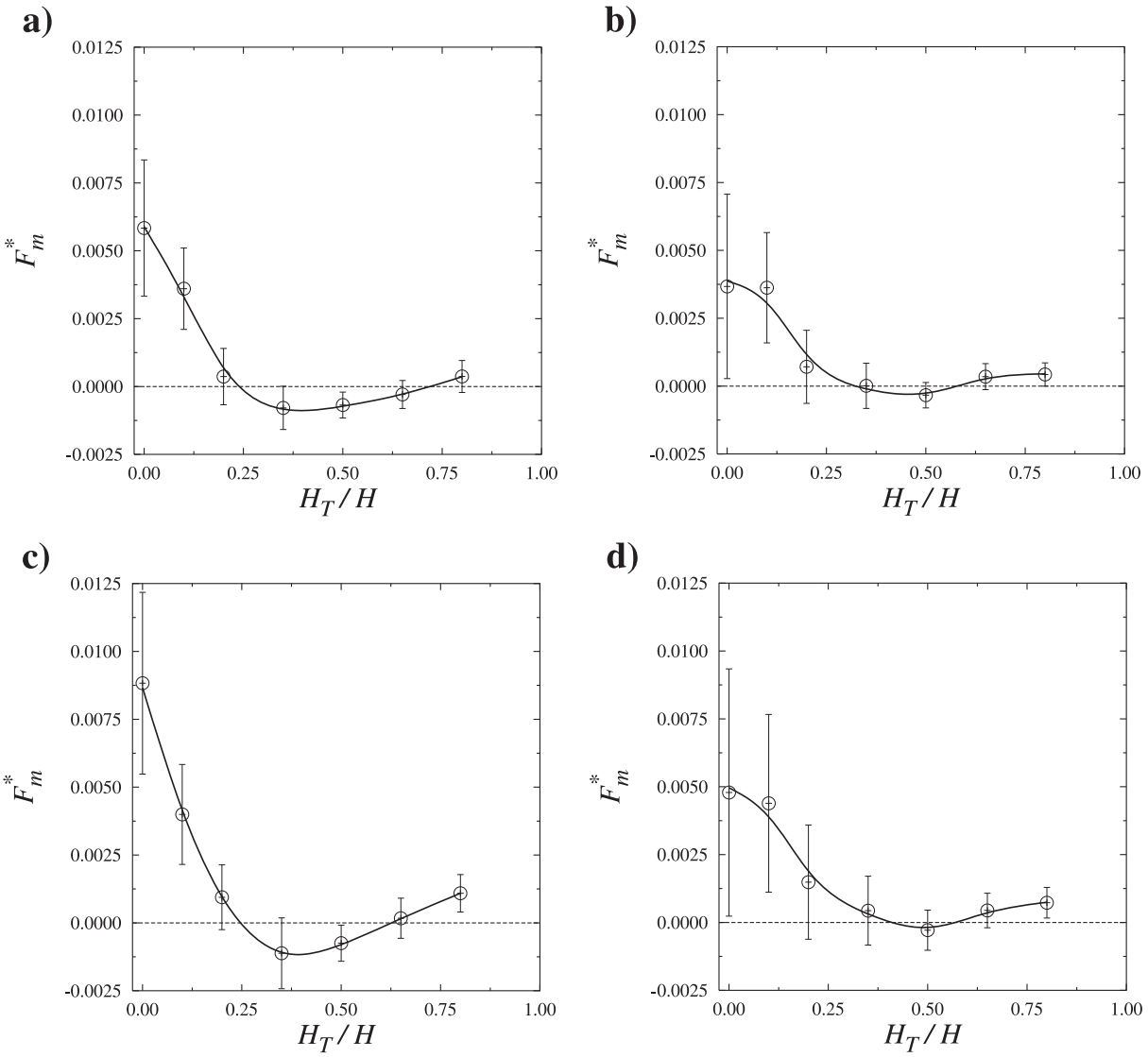

Fig. 2: Vertical distribution of mean dimensionless tangential force F_m^* and its standard deviation in a mixing vessel. Empty circles denote mean values; error bars depict interval of mean value ± one standard deviation: **a)** 4 blade impeller, $H_2/H = 0.2$; **b)** 4 blade impeller, $H_2/H = 0.35$; **c)** 6 blade impeller, $H_2/H = 0.2$; **d)** 6 blade impeller, $H_2/H = 0.35$.

ler number values. Examples are shown in Fig. 3, where the power spectra of the data measured at the lowest position of the measuring target ($H_T/H = 0$) are depicted. The heights of the MI-related peaks decrease with increasing ReM, but the peaks are easily detectable even at the highest ReM values used in the experiments. Fig. 3 further suggests that the dimensionless frequency $f_{MI}/f_M \approx 0.075$ corresponding to the maxima of the MI-related peaks does not depend on the impeller speed, the number of impeller blades and the impeller off-bottom clearance.

In order to analyse this presumption in greater detail, the dimensionless peak frequencies f_{MI}/f_M were determined for each data set, and then averaged values and standard deviations were evaluated. The results are summarised in Table 2. The peak frequencies take practically the same value for all vessel configurations. The magnitude of the differences of mean peak frequencies between configurations is comparable with the magnitudes of their standard deviation (the coefficient of variation takes values of about 10 % in all cases). The differences are not therefore significant. Nevertheless, we can speculate that the dimensionless frequency f_{MI}/f_M increases somewhat with an increasing number of impeller blades. The dependencies of the frequency of the MI-related peaks in the power spectra on the frequency of the impeller revolution and on the axial position along the baffle are shown in Figs. 4 and 5.

Fig. 4 shows f_{MI}/f_M values averaged along the baffle, i.e., averaged across all moving target positions H_T/H, as a function of the frequency of the impeller revolution. Full lines in Fig. 4 indicate the overall mean values from Table 2, and the dashed lines delimit the interval of the two standard deviations. It is evident that the f_{MI}/f_M value does not depend on

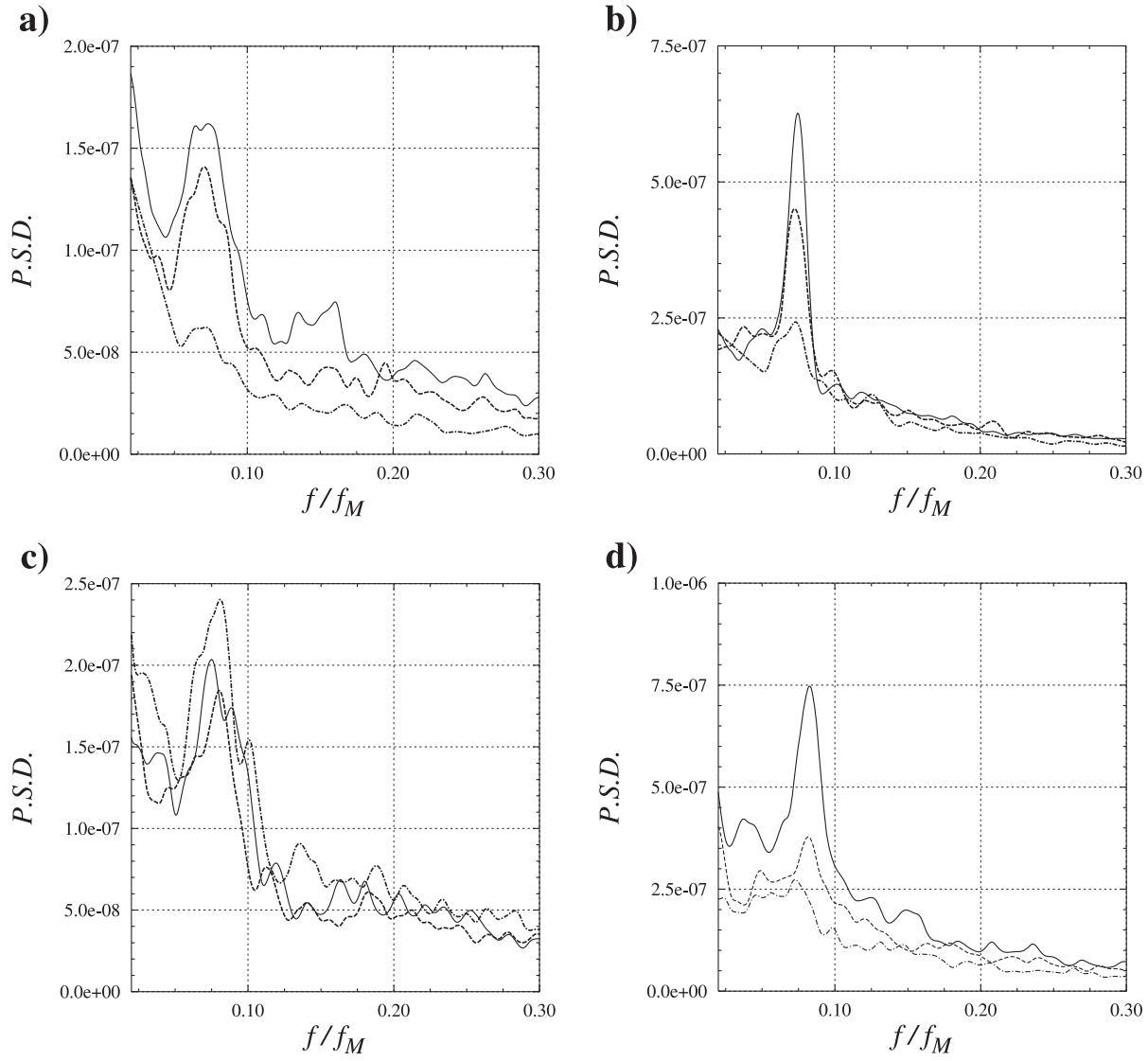

Fig. 3: Power spectral densities of tangential force measured at vessel bottom, $H_T/H = 0$: **a)** 4 blade impeller, $H_2/H = 0.2$; **b)** 4 blade impeller, $H_2/H = 0.35$; **c)** 6 blade impeller, $H_2/H = 0.2$; **d)** 6 blade impeller, $H_2/H = 0.35$. Full lines: $Re_M \approx 16000$; dotted lines: $Re_M \approx 25000$; dash-dotted lines: $Re_M \approx 50000$.

the impeller speed and on the viscosity of the working liquid. The dependencies of the f_{MI}/f_M values (averaged over all Re_M values) on target height depicted in Fig. 5 indicate that the f_{MI}/f_M value also does not depend on the axial position in the vessel. This fact confirms the deductions reported in the literature [7–10, 13–18, 21] that the macro-instability of the flow-pattern is a large-scale, spatially synchronised phenomenon occupying a substantial part of the mixing vessel volume. The results of frequency analysis indicate that the frequency of the macro-instability related component of tangential force f_{MI} increases linearly with increasing impeller speed f_M, as observed, e.g., by Brůha et al [7] and Montes et al [8–10]. The overall mean value of the proportionality constant between f_{MI} and f_M (resulting from our analysis, cf. Table 2) is 0.074. This value agrees well with the values reported by other authors [7–10, 15], although they used qualitatively different experimental data, for example local liquid velocity.

Quantification of the relative contribution of the MI-related component to the total tangential force affecting the baffle was performed by means of proper orthogonal decomposition of the experimental time series, as described in section 3. The used length of the N-window was $N = 300$. POD analysis unveiled a quite complex inner structure of the

Table 2: Mean values of dimensionless frequency f_{MI}/f_M of macro-instability related component of dimensionless tangential force affecting the baffle

N_B	H_2/H	Mean value	SD	CV
4	0.20	0.0691	0.0081	0.117
4	0.35	0.0718	0.0057	0.079
6	0.20	0.0765	0.0078	0.102
6	0.35	0.0775	0.0077	0.099

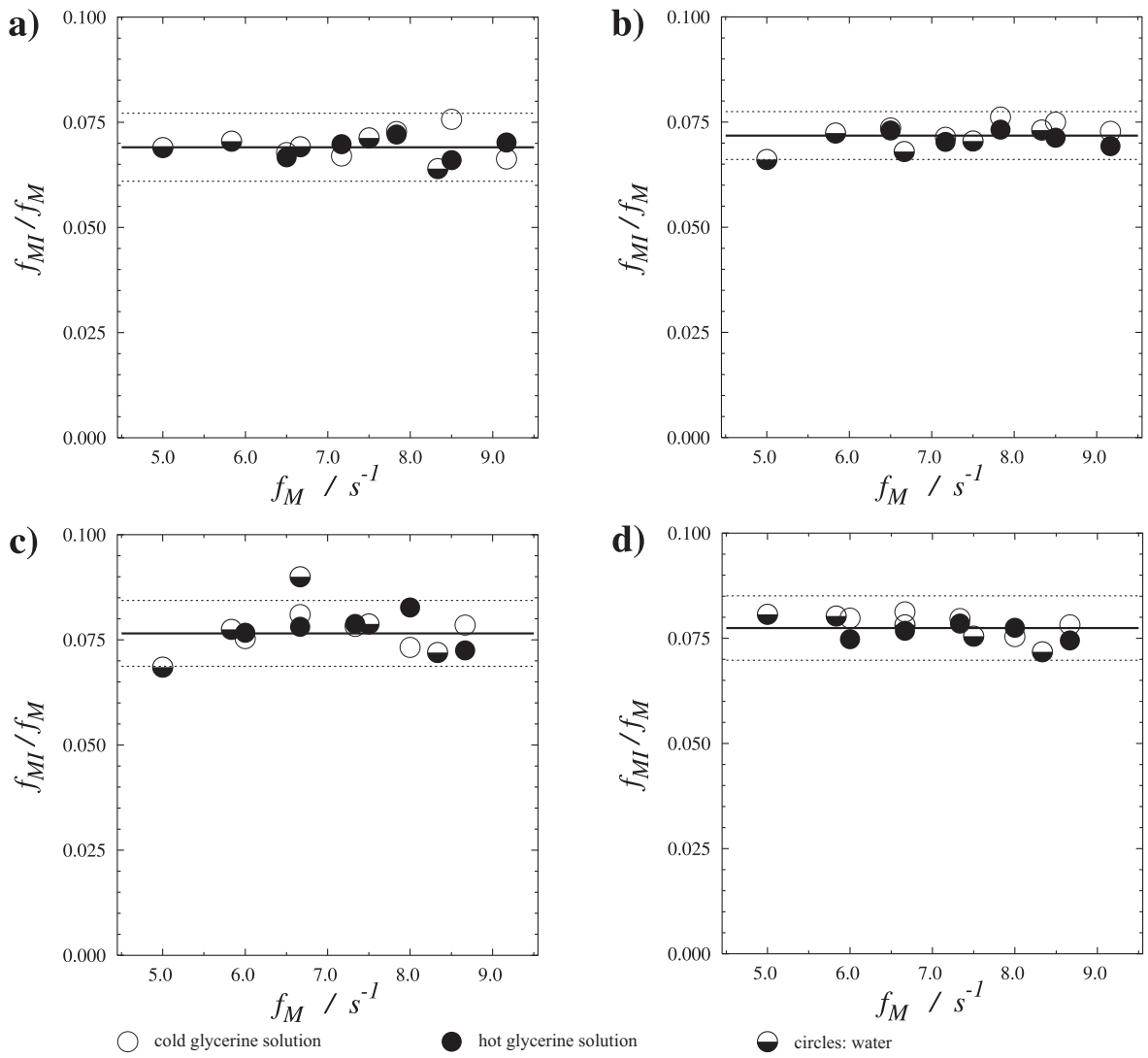

Fig. 4: Dimensionless frequency f_{MI}/f_M of macro-instability related fraction of the total tangential force averaged along the vessel height as a function of frequency of impeller rotation f_M: **a)** 4 blade impeller, $H_2/H = 0.2$; **b)** 4 blade impeller, $H_2/H = 0.35$; **c)** 6 blade impeller, $H_2/H = 0.2$; **d)** 6 blade impeller, $H_2/H = 0.35$. Full line: mean value; dashed lines: mean value ± one standard deviation.

low-frequency domain of the force: the spectrum of POD eigenvalues in Fig. 6 documents that the values of α_k decay quite slowly with increasing index k, i.e., the total force is composed of a large number of significant components. There is typically one leading (maximum) eigenvalue ($k = 1$) followed by 7–9 medium-valued eigenvalues ($k = 2$–10) capturing the low-frequency components of the force and, finally, there is a tail of slowly decaying low-valued eigenvalues ($k > 10$) capturing the high-frequency (turbulent and noisy) components of the force.

The leading eigenvalue α_1 reflects the presence of a very slowly varying component in the measured signal. Its dimensionless frequency is of the order of 10^{-4}–10^{-3} (substantially below the typical dimensionless MI frequency: 10^{-2}) and can be assigned to the unsteadiness of the operational conditions of the vessel or of the measuring equipment. The tail parts of the POD eigenvalue spectra in Fig. 6 correspond to eigenmodes with frequencies considerably above the typical MI frequency. These eigenmodes capture the fast, low spatial scale liquid motions (turbulent eddies) in the vessel. The macro-instability component of the total tangential force is typically captured by one or two (exceptionally by three) of the medium-valued eigenvalues ($k = 2$–10). This is documented in Fig. 7, where the power spectrum of the measured force is plotted (thick full line) together with the power spectra of the first ten POD eigenmodes. Two eigenmodes (specifically eigenmodes with $k = 2$ and $k = 3$) contribute to the MI component as their sole peaks (emphasised by empty and filled circles in Fig. 7) are located at exactly the same frequency as the MI-related peak in the spectrum of measured (non-decomposed) force. Other eigenmodes ($k \geq 4$) do not contribute to the MI component, as their peaks (plotted with dashed lines) do not coincide with the MI peak of total force, but are evenly spread across the low-frequency domain. Their peak frequencies are either lower or higher than f_{MI}, but do not coincide with f_{MI}. The relative magnitude Q_{MI} of the MI fraction of the total force was evaluated using Eq. (8) with $K_{MI} = \{2, 3\}$. In this way all data sets were processed and the Q_{MI} values were evaluated for all experimental configurations. The results are plotted in Figs. 8 and 9.

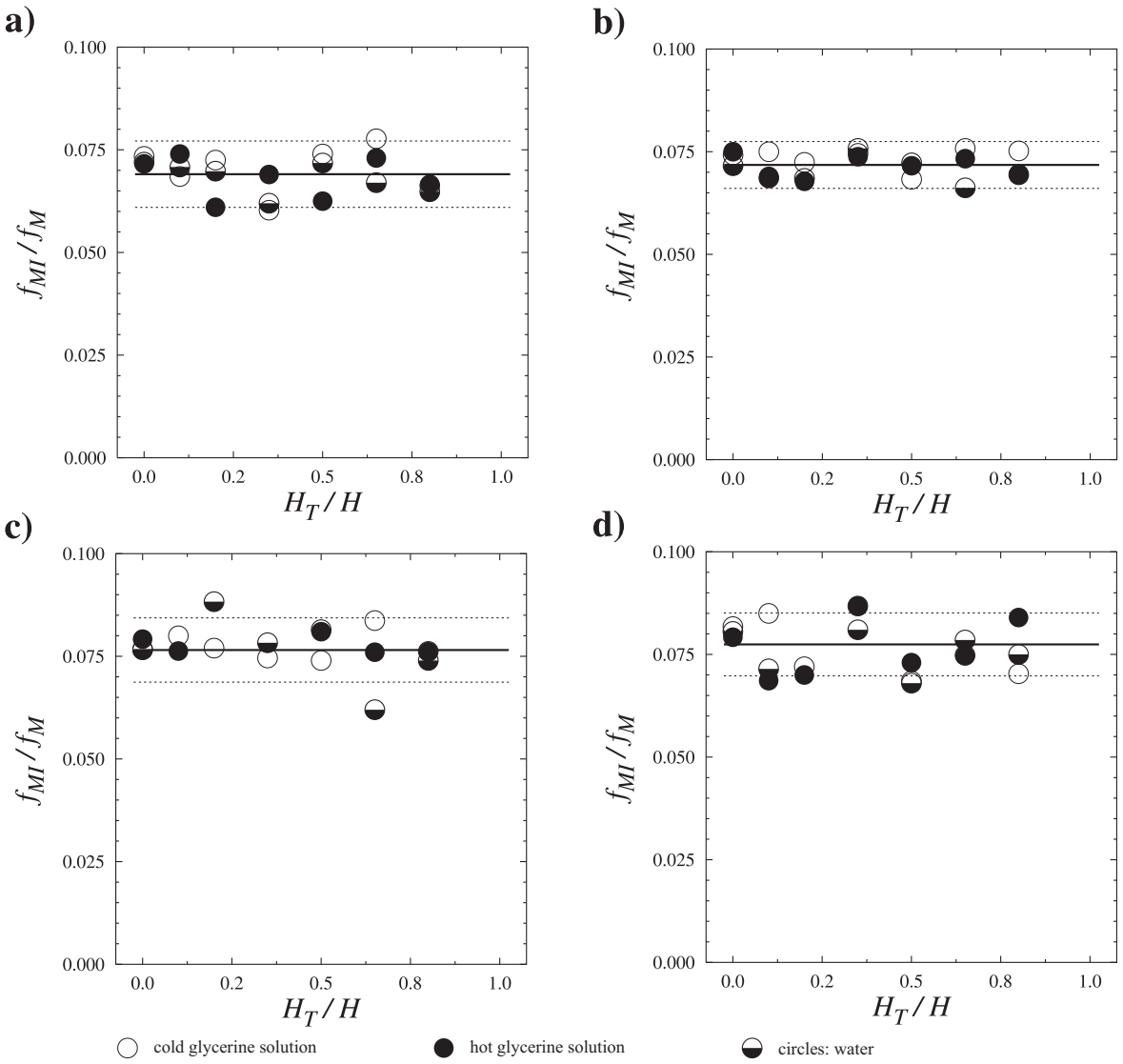

Fig. 5: Dimensionless frequency f_{MI}/f_M of macro-instability related fraction of total tangential force averaged over impeller rotation speeds as a function of dimensionless axial position H_T/H: **a)** 4 blade impeller, $H_2/H = 0.2$; **b)** 4 blade impeller, $H_2/H = 0.35$; **c)** 6 blade impeller, $H_2/H = 0.2$; **d)** 6 blade impeller, $H_2/H = 0.35$. Full line: mean value; dashed lines: mean value ± one standard deviation.

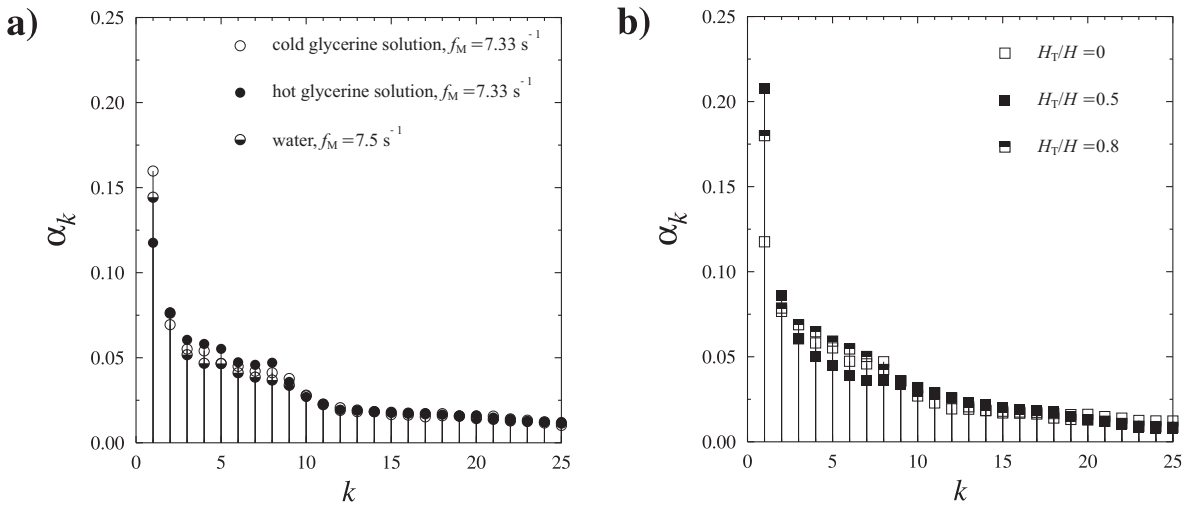

Fig. 6: Spectra of POD eigenvalues α_k obtained by POD of experimental tangential force time series. 6 blade impeller, off-bottom clearance $H_2/H = 0.2$: **a)** $H_T/H = 0$ (vessel bottom); **b)** $f_M = 7.33\ s^{-1}$, hot glycerine solution

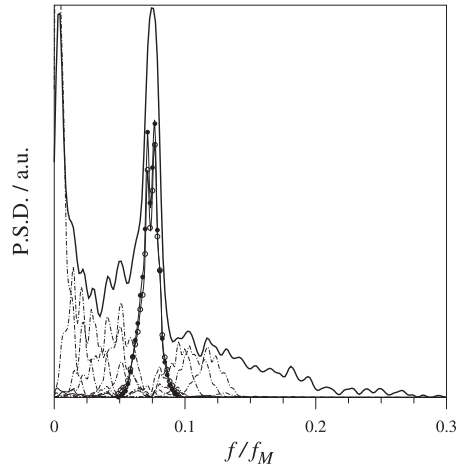

Fig. 7: Power spectral densities of measured tangential force (thick full line) and of its POD eigenmodes: the only POD eigenmodes #2 and #3 (thin full lines with filled and empty circles) contribute to the MI-related fraction of the total force. Other POD eigenmodes (thin dash-dotted lines) do not contribute to MI. Experimental conditions: 4 blade impeller; $H_2/H = 0.35$; $H_T/H = 0$; $f_M = 6.5\ s^{-1}$; $Re_M = 16818$ (cold glycerine solution).

The relative magnitude Q_{MI} of the MI-related component of the tangential force varies, in general, within the interval 0.05–0.15. These figures indicate that the macro-instability of the flow pattern in mixing vessels generates a significant part of the force effects exerted by a flowing liquid on solid surfaces, in this case on baffles. The primary factor affecting the value of Q_{MI} (cf. Figs. 8 and 9) is the impeller off-bottom clearance H_2/H. The principal effect of impeller off-bottom clearance on the circulation pattern in a stirred tank was demonstrated by Kresta and Wood [5]. The relative magnitude Q_{MI} of the MI component is markedly higher for higher impeller location $H_2/H = 0.35$.

The influence of impeller speed f_M on the value of Q_{MI} is weak (cf. Fig. 8): the Q_{MI} value decreases only modestly with increasing frequency of impeller revolution f_M. It can be concluded that the macro-instability related force affecting the baffles is a persistent phenomenon that is not destroyed by turbulent liquid flow in the vessel. The plots in Fig. 8 do not indicate any substantial and consonant influence of liquid viscosity on the Q_{MI} value, as the scatter of data points plotted in Fig. 8 is within the error limits of the Q_{MI} value evaluation.

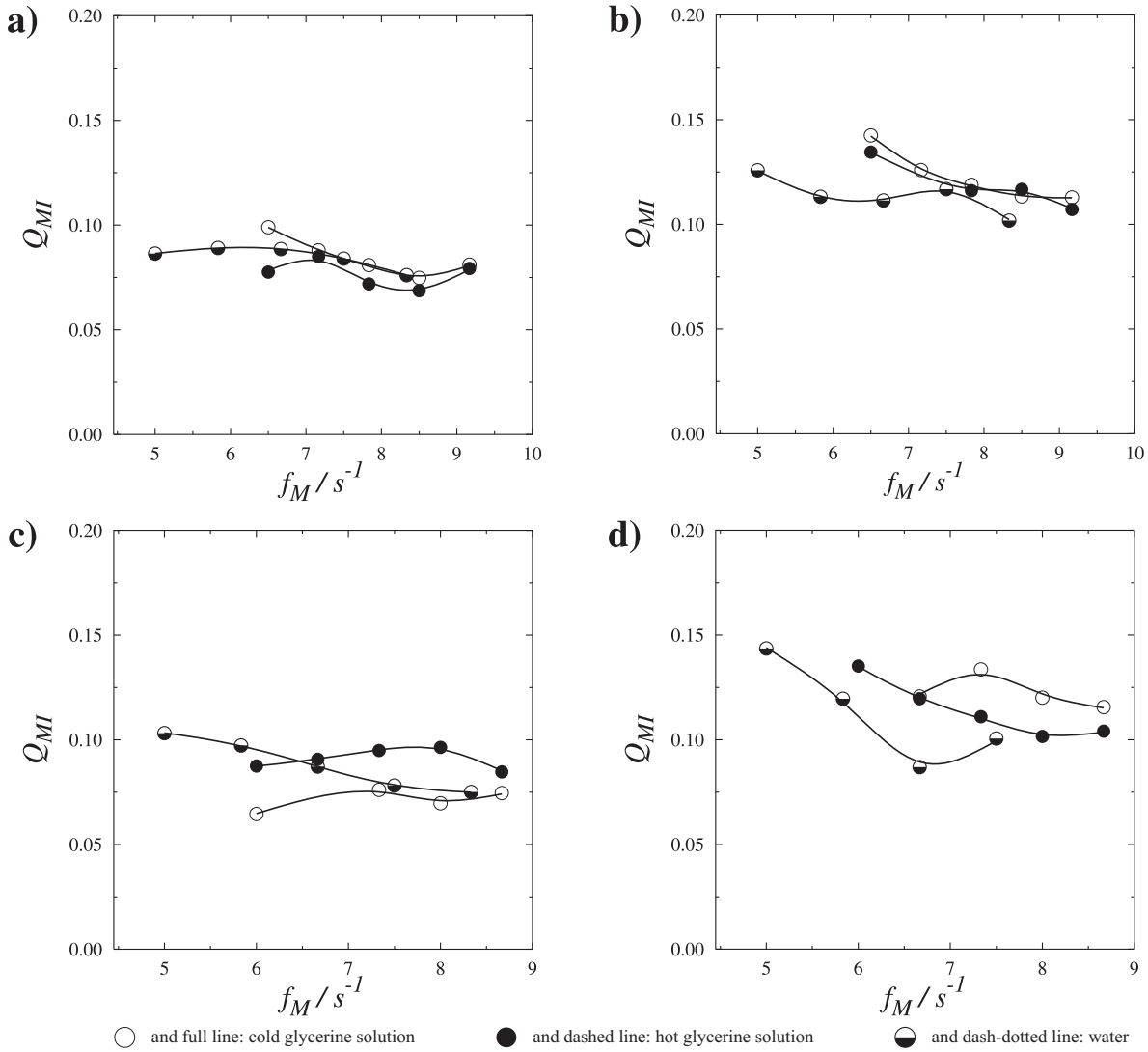

Fig. 8: Relative magnitude Q_{MI} of the MI-related fraction of the total tangential force affecting the baffle as a function of the impeller speed f_M: a) 4 blade impeller, $H_2/H = 0.2$; b) 4 blade impeller, $H_2/H = 0.35$; c) 6 blade impeller, $H_2/H = 0.2$; d) 6 blade impeller, $H_2/H = 0.35$. The points plotted at the same f_M value were obtained at distinct H_T/H values.

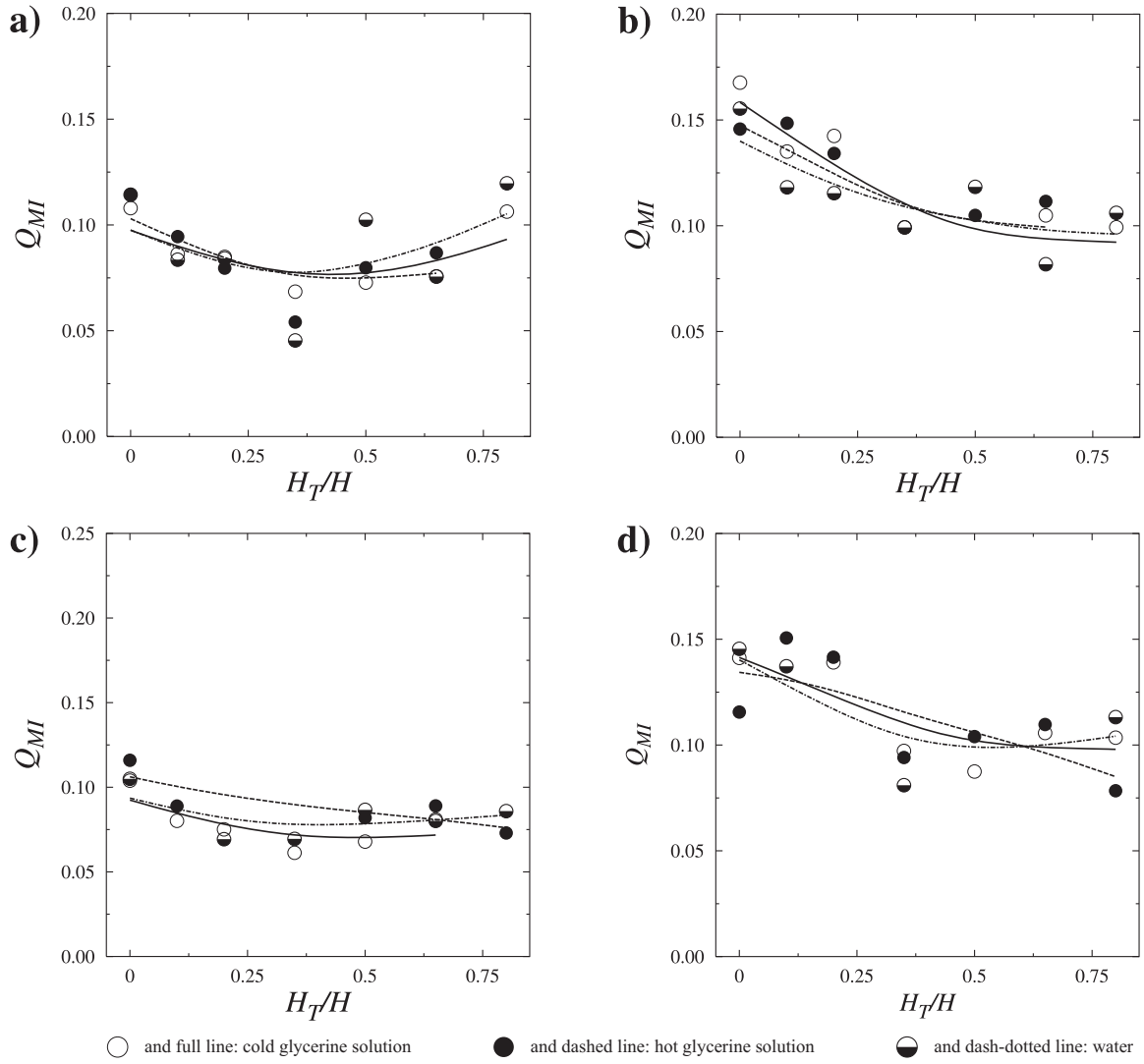

Fig. 9: Vertical distribution of the relative magnitude Q_{MI} of the MI-related fraction of the total tangential force: **a)** 4 blade impeller, $H_2/H = 0.2$; **b)** 4 blade impeller, $H_2/H = 0.35$; **c)** 6 blade impeller, $H_2/H = 0.2$; **d)** 6 blade impeller, $H_2/H = 0.35$

No effect of the number of impeller blades on the Q_{MI} value is visible.

The magnitude of the macro-instability related component of the tangential force varies significantly in the vertical direction (Fig. 9). The Q_{MI} value is, in general, higher at the vessel bottom, $H_T/H = 0$. This fact becomes very obvious when the impeller location is higher ($H_2/H = 0.35$) – cf. panels b) and d) in Fig. 9. When the impeller location is lower ($H_2/H = 0.20$), no monotonous dependence of the Q_{MI} value on the vertical position is obvious, but the decreasing trend of the Q_{MI} value with increasing vertical position still can be deduced, having in mind that the relative error of Q_{MI} evaluation is about ±15 %. Fig. 9 confirms the conclusions deduced from Fig. 8: the Q_{MI} value is substantially influenced by the impeller off-bottom clearance and by the number of impeller blades (higher values of both quantities invoke higher Q_{MI} values); liquid viscosity has only marginal effects on the Q_{MI} value.

5 Conclusions

The existence of macro-instability of the flow pattern in stirred vessels has been noted many times in the literature, but few attempts have been made to evaluate its quantitative measures. Recently we described a method for evaluating the relative magnitude of the MI-related component of the local liquid velocity [13, 14, 21]. In this paper the procedure was adopted for an analysis of qualitatively distinct data – the force affecting radial baffles in a stirred vessel. The procedure proved to be an efficient and reliable tool. The frequency of the MI-related component of the force and its relative magnitude were determined. The frequency of the MI-related component is independent of the operating conditions in the vessel and geometrical configuration of the vessel and the stirrer. The MI-related component forms a significant part of the total tangential force affecting the baffle.

Acknowledgement

This project was supported by the Ministry of Education of the Czech Republic (Projects: MSM223400007 and J04/98:212200008).

List of Symbols

$a(t)$	POD eigenmode	-
b	baffle width	m
B	moving target width	m
D	impeller diameter	m
f_M	frequency of impeller revolution	s^{-1}
f_{MI}	frequency of macro-instability	s^{-1}
F	tangential force affecting baffles	N
F^*	dimensionless tangential force affecting baffles	-
F_m^*	mean dimensionless force	-
h	impeller blade width	m
h_T	moving target height	m
H	liquid filling height	m
H_2	impeller off-bottom clearance	m
H_T	moving target axial position	m
N_B	number of impeller blades	-
N_S	number of samples	-
Q_{MI}	relative magnitude of MI-related fraction of tangential force	-
$\mathbf{R}$	autocovariance matrix	-
Re_M	impeller Reynolds number $Re_M=(f_M D^2 \rho)/\eta$	-
t	time	s
T	mixing vessel diameter	m
T_S	sampling period	s
$\mathbf{V}$	POD eigenvectors	-
$\mathbf{W}$	trajectory matrix	N
α	POD eigenvalue	-
ρ	liquid density	$kg\ m^{-3}$
η	dynamical liquid viscosity	Pa s
Φ^*	centred value of tangential force	N
$\mathbf{\Phi}^*$	vector of centred values of tangential force	N

Abbreviations

A/D	analog to digital conversion
CV	coefficient of variation
LDV	laser Doppler velocimetry
MI	macro-instability
POD	proper orthogonal decomposition
PSD	power spectral density
SD	standard deviation

References

[1] Bakker, A., Van den Akker, H. E. A.: *Gas-liquid contacting with axial flow impellers*. Transactions of the Institution of Chemical Engineers, 72A, 1994, p. 573–582.

[2] Bakker, A., Van den Akker, H. E. A.: *Single-phase flow in stirred reactors*. Transactions of the Institution of Chemical Engineers, 72A, 1994, p. 583–593.

[3] Chapple, D., Kresta, S.: *The effect of geometry on the stability of flow patterns in stirred tanks*. Chemical Engineering Science, 21, 1994, p. 3651–3660.

[4] Haam, S., Brodkey, R. S., Fasano, J. B.: *Local heat transfer in a mixing vessel using heat flux sensors*. Industrial and Engineering Chemistry Research, 31, 1992, p. 1384–1391.

[5] Kresta, S. M., Wood, P. M.: *The mean flow field produced by a 45° pitched blade turbine: changes in the circulation pattern due to off-bottom clearance*. Canadian Journal of Chemical Engineering, 71, 1993, p. 42–53.

[6] Winardi, S., Nagase, Y.: *Unstable phenomenon of flow in a mixing vessel with a marine propeller*. Journal of Chemical Engineering of Japan, 24, 1991, p. 243–249.

[7] Brůha, O., Fořt, I., Smolka, P., Jahoda, M.: *Experimental study of turbulent macro-instabilities in an agitated system with axial high-speed impeller and with radial baffles*. Collection of Czechoslovak Chemical Communications, 61, 1996, p. 856–867.

[8] Montes, J.-L., Boisson, H.-C., Fořt, I., Jahoda, M.: *Local study of velocity field macro-instabilities in mechanically agitated fluids in a mixing vessel*. 12th International Congress CHISA'96, Praha, Aug. 25–30, 1996.

[9] Montes, J.-L.: *Etude experimentale des fluctuations de vitesse de basse frequence dans une cuve agitee axialement*. PhD Thesis, Institut National Polytechnique de Toulouse, 1997.

[10] Montes, J.-L., Boisson, H.-C., Fořt, I., Jahoda, M.: *Velocity field macro-instabilities in an axially agitated mixing vessel*. Chemical Engineering Journal, 67, 1997, p. 139–145.

[11] Guillard, F., Träg rdh, C., Fuchs, L.: *New Image Analysis Methods for the Study of Mixing Patterns in Stirred Tanks*. The Canadian Journal of Chemical Engineering, 78, 2000, p. 273–285.

[12] Guillard, F., Träg rdh, C., Fuchs, L.: *A Study on the Instability of Coherent Mixing Structures in a Continuously Stirred Tank*. Chemical Engineering Science, 55, 2000, p. 5657–5670.

[13] Hasal, P., Montes, J.-L., Boisson, H.-C., Fořt, I.: *Macro-instabilities of velocity field in stirred vessel: detection and analysis*. Chemical Engineering Science, 55, 2000, p. 391–401.

[14] Hasal, P., Fořt, I.: *Macro-instabilities of the Flow Pattern in a Stirred Vessel: Detection and Characterization Using Local Velocity Data*. Acta Polytechnica, 2000, Vol. 40, p. 55–67.

[15] Bittorf, K. J., Kresta, S. M.: *Active volume of mean circulation for stirred tanks agitated with axial impellers*. Chemical Engineering Science, 55, 2000, p. 1325–1335.

[16] Kratěna, J., Fořt, I., Růžička, M., Brůha, O.: *Analysis of dynamic stress affecting a radial baffle in a mechanically agitated system*. Acta Polytechnica, 1999, Vol. 39, p. 11–38.

[17] Kratěna, J., Fořt, I., Brůha, O., Pavel, J.: *Local dynamic effect of mechanically agitated liquid on a radial baffle*. In: "Proceedings of the 10th European Conference on Mixing" (Editors: H. E. A. van den Akker and J. J. Derksen), Amsterdam, Elsevier 2000, p. 369–376.

[18] Kratěna, J., Fořt, I., Brůha, O., Pavel, J.: *Distribution of dynamic pressure along a radial baffle in an agitated system with standard Rushton turbine impeller*. Transactions of the IChemE, 79A, 2001, p. 819–823.

[19] Letellier, C., Le Sceller, L., Gousbet, G., Lusseyran, F., Kemoun, A., Izrar, B.: *Recovering deterministic behavior from experimental time series in mixing reactor*. A. I. Ch. E. Journal, 43, 1997, p. 2194–2202.

[20] Kovacs, T., Träg rdh, C., Fuchs, L.: *Fourier spectrum to recover deterministic and stochastic behavior in stirred tanks*. A. I. Ch. E. Journal, 47, 2001, p. 2167–2176.

[21] Hasal, P., Montes, J.-L., Boisson, H., Fořt, I.: *Macro-instabilities of velocity field in stirred vessel: detection, analysis and modeling*. 13th International Congress CHISA'98, Prague, August 23–28, 1998.

[22] Lumley, J. L.: *Stochastic tools in turbulence*. New York: Academic Press, 1970.

[23] Hožič, M., Stefanovska, A.: *Karhunen – Ločve decomposition of peripheral blood flow signal*. Physica A, 280, 2000, p. 587–601.

[24] Aubry, N., Guyonnet, R., Lima, R.: *Spatiotemporal analysis of complex signals: Theory and applications*. Journal of Statistical Physics, 64, 1991, p. 683–739.

[25] Broomhead, D. S., King, G. P.: *Extracting qualitative dynamics from experimental data*. Physica D, 20, 1986, p. 217–236.

[26] Kolodner, P., Slimani, S., Aubry, N., Lima, R.: *Characterization of dispersive chaos and related states of binary fluid convection*. Physica D, 85, 1995, p. 165–224.

[27] Press, W. H., Teukolsky, S. A., Vetterling, W. T., Flannery, B. P.: *Numerical Recipes in FORTRAN*. Cambridge: Cambridge University Press, 1992.

Doc. Ing. Pavel Hasal, CSc.
phone: +420 224 353 167
fax: +420 233 337 335
e-mail: Pavel.Hasal@vscht.cz

Institute of Chemical Technology, Prague
Department of Chemical Engineering & Center for Nonlinear Dynamics of Chemical and Biological Systems
Technická 5
166 28 Praha 6, Czech Republic

Ing. Jiří Kratěna
phone: +420 224 352 713
e-mail: kratena@student.fsid.cz

Doc. Ing. Ivan Fořt, DrSc.
phone: +420 224 352 713
fax: +420 224 310 292
e-mail: fort@fsid.cvut.cz

Dept. of Process Engineering
Czech Technical University
Faculty of Mechanical Engineering
Technická 4
166 07 Praha 6, Czech Republic